CALCULATION OF THE POINT IMAGE DIFFUSION FUNCTION FOR AN ADAPTIVE TELESCOPE WITH A HARTMANN WAVE–FRONT SENSOR

V.P. Lukin, N.N. Mayer, and B.V. Fortes

Institute of Atmospheric Optics,
Siberian Branch of the Russian Academy of Sciences, Tomsk
Received October 1, 1992

An adaptive telescope with a Hartmann sensor of the wave–front distortions and a phase corrector in the form of a matrix of square–shaped segments is considered. The efficiencies of two algorithms of the corrector control are compared. One of the proposed algorithms is very simple and can be performed without a processor, i.e., with an analog device and hence can provide fast response at a low cost of a corrector control unit. The other algorithm is based on a model representation of the wave–front distortions and uses the least–squares method for seeking for coefficients at the aberration polynomials. The latter algorithm needs for a processor, but provides a diffraction–limited resolution at a sufficient level of the reference signal. The function of the point image diffusion has been calculated for both methods. The averaging was done over random samples of the wave–front distortions generated on a computer.

1. INTRODUCTION

The problem in reconstructing of the shape of optical radiation front with the use of a phase difference was investigated in a number of papers.[12–23] The authors of these papers have studied the influence of uncorrelated additive noises (for example, photon noise) interfering the estimations of phase differences or wave–front gradients, and the restoration of a phase at a discrete set of points. However, all these works excluding Ref. 22 neglect a specific character of an instrumental error introduced by the Hartmann wave–front sensor into the estimate of the phase difference. In Ref. 22 the Hartmann sensor is considered as a device measuring the displacements of the wave–front fragments of an optical beam focused by subapertures. However, in this work a particular case of the sensor design is considered, in which the displacements are estimated from the differences of energies incident upon the upper (lower) and left (right) halves of four square–shaped photodetectors positioned in the focal plane of the sensor, while the aberrations of the wave front on the subaperture are neglected.

In this paper we calculate numerically the point image diffusion function (PIDF) of an adaptive telescope implementing the program which simulates its basic components such as the wave–front sensor (of the Hartmann–type sensor) and a segmented corrector composed of a matrix of the square–shaped elements. Distribution of the intensity over the focal plane of each subaperture was calculated in the paraxial approximation thus allowing for the diffraction and aberration of the wave front. The photon noise was simulated with the help of a sensor generating a sequence of random numbers distributed according to the Poisson law. Then the program calculated the displacements of the center of gravity of the intensity distribution over the focal plane of each subaperture with respect to its diffraction position and determined the tilts and the displacements for each corrector element with the help of the algorithms

mentioned above. The corrected wave front was used for calculating a short–exposure PIDF, which was averaged over the random samples of turbulent distortions.

Such an approach allows one to simultaneously account for different factors introducing the errors not only into the measurements but also into the correction of distortions of the wave front as well as to obtain the final result in terms of the PIDF and, if necessary, in terms of the optical transfer function. The sources of measurement errors are, in particular, the aberrations of a wave front on the sensor subapertures caused by the atmospheric turbulence of small scales. Such errors no longer can be regarded as uncorrelated as is in the case of the photon noise. In addition, with increase of the number of subapertures the aberrations of the wave front on an individual subaperture decrease and the spatial resolution of the sensor becomes higher, whereas the uncertainties due to the quantum intensity fluctuations increase. Thus, the efficiency of a correction depends in a complicated way on the number of subapertures, strength of turbulent disturbances, and signal intensity.

2. TECHNIQUE FOR CALCULATING THE TURBULENT PIDF

Random turbulent distortions of the wave front were simulated using the approximation of a phase screen placed in the aperture plane of a telescope. A two–dimensional spectral density of the phase fluctuations of a plane wave for the case of light propagation in the atmosphere, being described in the approximation of geometric optics, has the form[1]

$$F_S(k) = 0.489 r_0^{-5/3}(k^2 + k_0^2)^{-11/6} , \qquad (1)$$

where

$$r_0 = (0.423 \, k^2 \int C_n^2(h) \, \mathrm{d}h)^{-3/5} \qquad (2)$$

is Fried's coherence parameter,[4,5] $k = 2\pi/\lambda$ is the wave number, $C_n^2(h)$ is the profile of the structure constant of the refractive index fluctuations along the propagation path, and $\kappa_0 = 2\pi/L_0$, L_0 is the outer scale of the turbulence. This latter parameter was taken to be equal to 100 m. The inner scale of the turbulence does not enter explicitly into the spectrum (Eq. (1)), however, in the numerical simulation of turbulent distortions the scales smaller than the grid step are lost and therefore the inner scale of the turbulence is taken to be equal to the grid's step. In our calculations the grid's step was about 2 cm.

Distortions of the wave front $S(x, y)$, complex amplitude $U(x, y)$, and the intensity $I(x, y)$ of the optical wave were represented in the form of two–dimensional arrays $S(l, m)$, $U(l, m)$, and $I(l, m)$, $l, m = 1, ..., N$ set on the X and Y coordinates over square grid with the step Δx and size N which covers the spatial region with the extension $G = N \cdot \Delta x$ along each of the coordinates. The random wave front $S(l, m)$ has been generated by two methods.

The first method based on the fast Fourier transform (FFT)[8,9,10] was used for simulating the random spatial fluctuations with the scales smaller than the region under investigation but larger than the grid step Δx. In other words, this method was used for generating the random wave front with the spectral density

$$F_1(x) = \begin{cases} 0, & 0 < k < k_{min}, \\ F_S(k), & k_{min} < k < k_{max}, \\ 0, & k_{max} < k < \infty, \end{cases} \tag{3}$$

where $\kappa_{min} = 2\pi/G$, $\kappa_{max} = \pi/\Delta x$. This restriction is associated with the fundamental property of the discrete Fourier transform, owing to which the frequency range is limited by the band $[\kappa_{min}, \kappa_{max}]$. For the spectrum F_S of the type given by Eq. (1) only the loss of large–scale fluctuations is of significance (provided that the diameter of the aperture is much larger than the inner scale of the turbulence that is true for the problem under study). In order to take into account the large–scale fluctuations we supplement the wave front $S_1(l, m)$, obtained using the FFT method, with the aberrations calculated by summing the first N_P Zernike polynomials[2,6,7]

$$S_2(l, m) = \sum_{q=2}^{N_P} a_q Z_q [(l - l_0)\Delta x, (m - m_0)\Delta y] \tag{4}$$

with the coefficients a_q which were generated as random numbers distributed normally with the zero mean and with the variances being equal to

$$\sigma_n^2 = 8\pi(n + 1) \int k \, dk \, F_2(k) \frac{J_{n+1}^2(kR)}{(kR)^2}, \tag{5}$$

where n is the radial power of the polynomial, R is the radius of a circle in which the polynomials $Z_q(x, y)$ are orthogonal, l_0 and m_0 are the coordinates of center of the circle, and F_2 is defined as

$$F_2(k) = \begin{cases} F_S(k), & k < k_{min} \\ 0, & k > k_{min} \end{cases}. \tag{6}$$

The number of polynomials N_P in sum (4) was taken to be 15 that corresponds to the polynomials of up to the fourth power.

Thus, the random phase screen is represented as the sum of two components

$$S(l, m) = S_1(l, m) + S_2(l, m) \tag{7}$$

in which the component S_2 was calculated as sum (4) with the random coefficients a_q, while S_1 was obtained as a result of calculation of the two–dimensional FFT of the array $A(l, m)$, $l, m = 1, ..., N$ which represented a random two–dimensional spectral amplitude set on the coordinates grid with the step $\Delta\kappa = 2\pi/G$. The array $A(l, m)$ was generated as the matrix of independent random complex numbers obeying the following conditions:

1) $|A(l, m)|^2 = F_1((l - 1) \Delta\kappa, \ (m - 1) \Delta\kappa) \Delta\kappa$, $l = 1, \ N_N$, $m = 1, \ N$;

2) $\arg (A(l, m)) = 2\pi$ RND, $l = 1, \ N_N$, $m = 1, \ N$;

3) $A(l, m) = A^*(N - 1, N - m)$ for the rest of l and m.

Here N_N is the number corresponding to the Nyquist frequency while the RND is the random number distributed uniformly within the interval [0, 1]. The first of these conditions ensures the correspondence of the spatial spectrum of each realization $A(l, m)$ to a preset two–dimensional spectral density, the second one ensures the randomness of realizations of the wave front distortions, and the third one is required for obtaining a purely real array $S(l, m)$ after making FFT calculations.

We calculated the distribution of a complex amplitude according to the obtained random realization of the wave front and then we found the intensity distribution over the focal plane of a converging lens. The lens aperture function was set to be equal to unity inside the square with the side $D = 1$ m and to be equal to zero outside it. The radius R for calculating the polynomials Z_q was taken to be equal to $D/2^{1/2}$. The field in the focus was calculated either as the Fourier transform of the initial complex amplitude (Fraunhofer diffraction) or in the paraxial approximation (Fresnel diffraction). In the latter case it is necessary to perform the FFT twice (direct and inverse transforms) and to multiply the spectrum of the focused field by the filtering function[3] corresponding to passing the focal length f after the first FFT. This method increases the amount of calculations by a factor of 2–3 but allows one to vary the focal length and to obtain the intensity distribution in the focal plane with an arbitrary angular step. The second method was used for calculating a corrected PIDF.

3. MODELING THE SENSOR AND THE CORRECTOR OF THE WAVE FRONT

In this paper we consider a segmented corrector of the wave front in the form of a matrix of square–shaped elements with the size $d = D/N_C^{1/2}$ (N_C is the number of corrector elements), being independently controlled along three degrees of freedom, that is tilts with respect to the X and Y axes and displacements along the Z axis. We assume that the corrector and aperture of the wave–front sensor are in the planes adjoint with the telescope aperture plane and hence the distortions of the wave front can be considered to be identical to those in the aperture plane.

The wave–front sensor is a matrix of converging lenses of the same shape, and size as the matrix of the corrector elements. In the focal plane of each sensor subaperture a distorted image of a monochromatic point source is formed. For each subaperture we calculated the intensity distribution over this image by the methods that we had used for calculating the PIDF of the telescope and then we obtained the intensity distribution in the plane of detectors in the form of a two–dimensional array $I_k(l, m)$, $l, m = 1, ..., N_d$, $k = 1$, N_S, where N_d is the size of the calculation grid used for calculating the intensity in the focal plane of a subaperture, $N_S = N_C$ is the number of subapertures being equal to the number of the corrector elements. Then we calculated deviations of the center of gravity of each image from its diffraction position

$$\mathbf{r}_k = \Delta x \, \frac{\left(\sum\limits_{l, m} I_k(l, m) \, (\mathbf{e}_x(l - l_0) + \mathbf{e}_y(m - m_0)) \right)}{\left(\sum\limits_{l, m} I_k(l, m) \right)} \, , \qquad (8)$$

where l_0 and m_0 are the coordinates of the center of gravity of the diffraction image, $\mathbf{e}_x$ and $\mathbf{e}_y$ are the unit vectors of the directions along the X and Y axes, respectively, Δx is the grid step in the plane of detectors, and $k = 1, ..., N_S$. The estimate of the wave front tilt averaged over the subaperture is related to the $\mathbf{r}_k$ value by the equation

$$\mathbf{g}_k = \mathbf{r}_k / f_H \, , \qquad (9)$$

where f_H is the distance between the plane of subapertures and that of the photodetectors of the Hartmann sensor.

For simulating the photon noise we transformed the array $I_k(l, m)$ into the array $P_k(l, m)$ according to the following rule:

$$P_k(l, m) = \text{RNDP} \left(N_{ph} / N_{S*} I_k(l, m) \, / \sum\limits_{l, m} I_k(l, m) \right), \qquad (10)$$

where N_{ph} is the statistically mean number of photons passed through the sensor aperture during the exposure time, $\text{RNDP}(I)$ is the random number distributed according to the Poisson law with the mean value being equal to I. Then we substituted the arrays P_k into formula (8) for I_k and thus obtained the noise estimates of the tilts $\mathbf{g}_k$. Thus, each element of the array P_k represented a random number of photons absorbed by the photodetector element with the size Δx by Δy centered at the point (l, m).

4. THE MODAL METHOD OF WAVE FRONT RECONSTRUCTION

The modal method of reconstructing wave fronts, we use in our study, is analogous to that studied in Refs. 16 and 19, where a detailed analysis of it is given. For this reason we give here only a brief formulation of the mathematical aspects of the problem. Thus, we assume that the wave front $S(x, y)$ can be represented sufficiently accurately as a finite sum of Zernike polynomials

$$S(l, m) = \sum\limits_{q=z}^{N_m} a_q \, Z_q \, ((l - l_0)\Delta x, \, (m - m_0)\Delta y] \, , \qquad (11)$$

where N_m is the number of polynomials used in the modal representation. The problem is to find the vector of the coefficients $\{a_q\}$ that minimizes the functional

$$F = \sum\limits_{k=1}^{N_S} \left(\mathbf{q}_k - \sum\limits_{q=2}^{N_m} a_q \, \hat{\mathbf{Z}}_{qk} \right)^2 \, , \qquad (12)$$

where $\hat{\mathbf{Z}}_{qk}$ is the gradient of the qth polynomial on the kth subaperture of the sensor. In Ref. 16 the gradients $\hat{\mathbf{Z}}_{qk}$ were calculated at the subaperture centers while in Ref. 19 the variant was considered of calculating the average over the whole subaperture gradient of the corresponding polynomial. We have used the latter method and determined the components of the vector $\hat{\mathbf{Z}}_{qk}$ as the coefficients of the equation of a plane approximating the polynomial $\mathbf{Z}_q$ on the kth subaperture. By solving the variational problem of minimazing the functional F, we obtain a system of linear equations which, in the matrix form, can be written as

$$\| W \| \, \| a_q \| = \| \mathbf{V} \| \, \| \mathbf{g}_k \| \, , \qquad (13)$$

where W is the N_m by N_m matrix while V is the N_m by N_S matrix. A solution of the system of linear equations (13) is

$$\| a_q \| = \| \mathbf{Q} \| \, \| \mathbf{g}_k \| \, , \qquad (14)$$

where the matrix $\mathbf{Q}$ of the N_m by N_S rank is related to the matrices W and $\mathbf{V}$ by the equation

$$\| \mathbf{Q} \| = \| W \|^{-1} \, \| \mathbf{V} \| \, . \qquad (15)$$

The obtained vector $\{a_q\}$ was used for calculating the displacements of segments of the corrector along the Z axis. To do this we preliminarily calculated the mean value $\tilde{Z}_{qk}$ of the polynomial Z_q on the area corresponding to the kth element of the corrector and then summed up these values with the weights a_q. Thus, the displacement of the kth element of the corrector is calculated by the formula

$$C_k = \sum\limits_q a_q \, \tilde{Z}_{qk} \, . \qquad (16)$$

To control the tilts of the corrector elements we directly used the estimates of an average, over the corresponding subaperture, value of the wave–front gradient. This is possible in our case because the number, size and arrangement of the elements of the corrector are the same as for the subapertures of the sensor.

Depending on the number of polynomials, and for $N_S = 16$ the time (in milliseconds) of calculation of the coefficients a_q and the displacements C_k with the use of the gradients g_k and precalculated matrix Q on a computer with the INTEL–80386 processor (with clock frequency of 25 MHz) was:

$N_{\rm m}$	3	6	10	15	21	28
time	3	5	7.5	11	15	20

this time increases approximately by a factor of four for $N_S = 64$

$N_{\rm m}$	3	6	10	15	21	28
time	9	17	27	39	54	72

5. ANALOG METHOD FOR RECONSTRUCTING THE WAVE FRONT

It should be first mentioned that in fact this analog method is not the measurement technique. It is rather a technique for the phase control or formation of the phase distribution using data of phase gradients measured by the Hartmann method.

In order to put this method into practice one should have a special controllable (active) mirror, the shape and size of an individual element of which completely coincide with those of a subaperture of a Hartmann meter which are taken in accordance with the input pupil of the optical system. Such a mirror belongs to the class of mirrors operating in the regime of zonal control. The reflecting surface of the mirror is composed of squared segments. The number of elements $N_{\rm E} = m_{\rm H}^2$, where $m_{\rm H}$ is the dimension of the Hartmann matrix.

The mirror has a multilayer structure. The first element (or layer) of the mirror serves as the base plate for the whole mirror, the second layer is the active element of the bimorph type rotating the whole mirror surface at angles whose values are calculated by averaging the data obtained with the use of the Hartmann sensor at all subapertures. The third layer is the active element rotating an individual segment of the mirror (in the case of square matrix each of these segments consists, in turn, of four individual elements) at the angles obtained by averaging the data of measurements over each of segments. Next controlling layer of mirror consists now of 16 segments. And further every subsequent layer is a set of active elements, controllable only with respect to the tilt. For the square Hartmann matrix the number of controlling layers of the mirror is equal to $1 + 1/2\log_2 N_{\rm E}$. Thus, if the number of elements in the Hartmann diaphragm is 64, then the mirror has 4 controlling layers.

It seems so that in the limiting case of dividing the mirror into a large number of controlling zones, it could be possible to describe in full detail the phase function (or the mirror surface) in terms of the tilts of the layers relative to each other.

Controlling over each layer within an individual element is calculated by a simple summation of measured local gradients of the phase minus the control at the preceding step.

6. PIDF IN THE CASE OF USING THE SEGMENTED CORRECTOR

In this section we shall present the results of calculations of the PIDF performed under the assumption that at each point of the aperture the distortions of wave front are known. For each element of the corrector the tilts and displacements were determined from the condition of minimizing the residual distortions of wave front by the least–squares method. The obtained PIDF's illustrate the restrictions associated only with the finite number of elements of a corrector.

Shown in Fig. 1 is the radial distribution $I(\rho)$ of the PIDF obtained by averaging the long exposure PIDF $I(\rho, \varphi)$ over the angle φ. Figure 1a presents the data obtained at $r_0 = 20$ cm ($D/r_0 = 5$), while Fig. 1b at $r_0 = 10$ cm ($D/r_0 = 10$). The number N_C of the corrector elements has varied from 1 to 64. Table I lists the values of the Strehl ratio (St) being equal to the ratio of the PIDF maximum to its diffraction value and full width of the PIDF at the level of half–maximum (English abbreviation is FWHM). Here and in the below consideration the wavelength λ is taken to be equal to 0.55 μm.
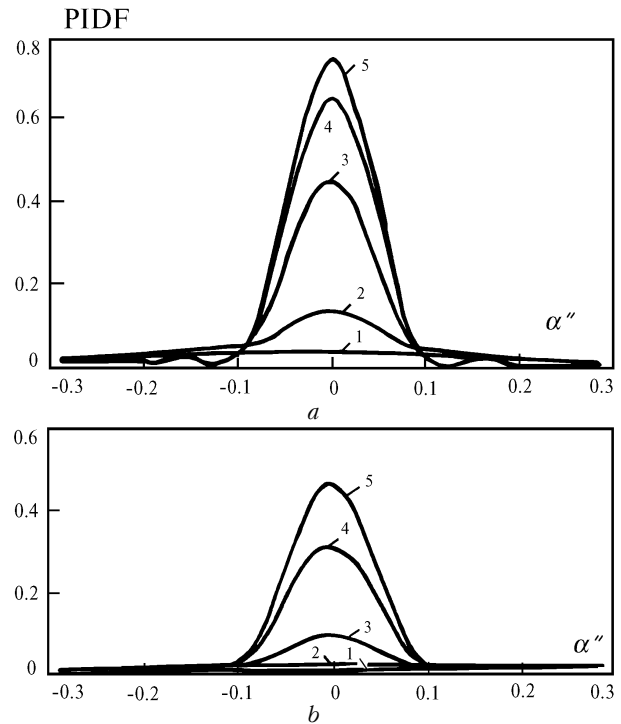
FIG. 1. The PIDF for ideally measured wave front distortions as a function of angular distance α when correcting the distortions by a segmented corrector: without any corrections (1), $N_C = 1$ (2) (correction of the common tilt), 4 (3), 16 (4), and 64 (5); $r_0 = 20$ cm (a), and $r_0 = 10$ cm (b).

TABLE I.

N_C	d/r_0	St	FWHM
	$r_0 = 20$ cm		
—	—	0.03	0.5″
1	5	0.13	0.14″
4	5/2	0.45	0.10″
16	5/4	0.67	0.09″
64	5/8	0.75	0.09″
	$r_0 = 10$ cm		
—	—	0.008	1.1″
1	10	0.017	0.64″
4	5	0.089	0.11″
16	5/2	0.31	0.10″
64	5/4	0.46	0.10″

Thus we can see, that the diffraction resolution (FWHM = 0.9″ for $D = 1$ m and $\lambda = 0.55$ μm) is reached already at the size of the corrector element equal approximately to 3–5 radii of coherence r_0. Further increase of the number of elements of a corrector results only in the intensity increase. This conclusion well agrees with the results obtained in Refs. 10 and 11 for a segmented corrector with hexagonal elements.

7. PIDF IN THE CASE OF A MODAL RECONSTRUCTION OF A WAVE FRONT

In this section we present the results of calculation of the PIDF of an adaptive telescope which uses the wave–front sensor of a Hartmann type and a segmented corrector of the wave front which is controlled according to the above–described algorithm of the modal reconstruction of the wave–front distortions.
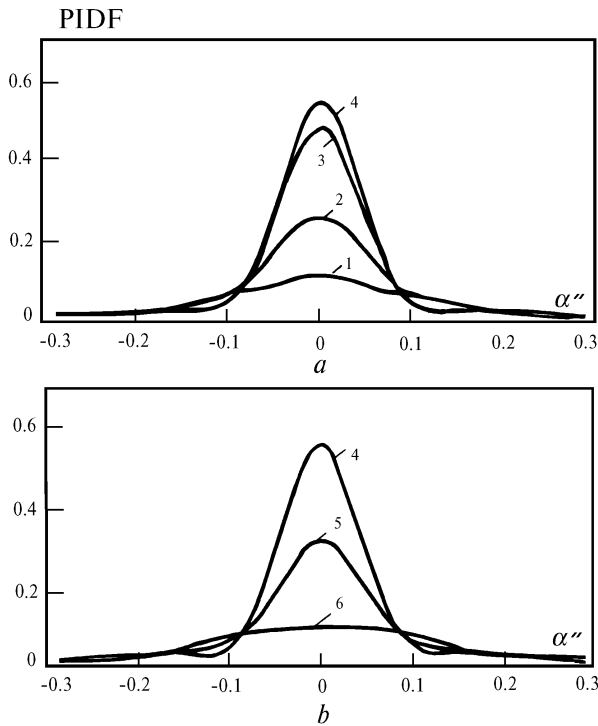
FIG. 2. PIDF value calculated using a modal algorithm of wave–front reconstruction for different numbers of polynomials N_m in the modal representation (11): $N_m = 3$ (1), 6 (2), 10 (3), 15 (4), 21 (5), and 28 (6); $r_0 = 20$ cm and $N_C = N_S = 16$.

Shown in Figs. 2a and 2b are the long exposure PIDF's obtained for $r_0 = 20$ cm and $N_S = 16$, while in Table II the corresponding values of the St parameter and the FWHM are listed. In Tables II and III marked by asterisks are the strings corresponding to the estimate of a local tilt according to the displacement of the center of gravity focused by the radiative subapertures. In other cases we used the least–squares method and calculated the tilt directly from the wave–front measurements. The number N_m of polynomials in the modal representation (Eq. (11)) of the wave front was 3, 6, 10, 15, 21 or 28,

that corresponds to the polynomials of the 1st, 2nd, 3rd, 4th, 5th or 6th orders, respectively. At $N_m = 21$ an increase in the error of wave–front reconstruction was observed. It appears to be caused by the effects discussed in Ref. 19. However, as can be seen from Fig. 2 and Table II, as early as at $N_m = 10$ the growth of the efficiency of the correction does not practically change. Thus, it appears that the amount of polynomials being equal to the number of the subapertures of the sensor is quite sufficient for a successful use of the algorithm of modal reconstruction of wave fronts.

TABLE II.

N_m	St	FWHM
3	0.11	0.20″
6	0.25	0.13″
10	0.47	0.10″
15	0.54	0.10″
15*	0.58	0.10″
21	0.30	0.11″
28	0.09	0.27″

8. PIDF FOR THE CASE OF ANALOG ALGORITHM OF A WAVE–FRONT RECONSTRUCTION

In this section we present the results of calculation of the PIDF with the use of analog algorithm of a wave–front reconstruction described in the preceding section. The number of the subapertures of the sensor and segments of the corrector were 4, 16 and 64. The calculational results are shown in Fig. 3 and in Table III. It can be seen, that although the quality of a correction is markedly worse than in the case of using the method of modal reconstruction of wave front, nevertheless the use of a sufficiently large number of subapertures of a sensor allows one to reach a multiple intensity increase as compared to the uncorrected PIDF.
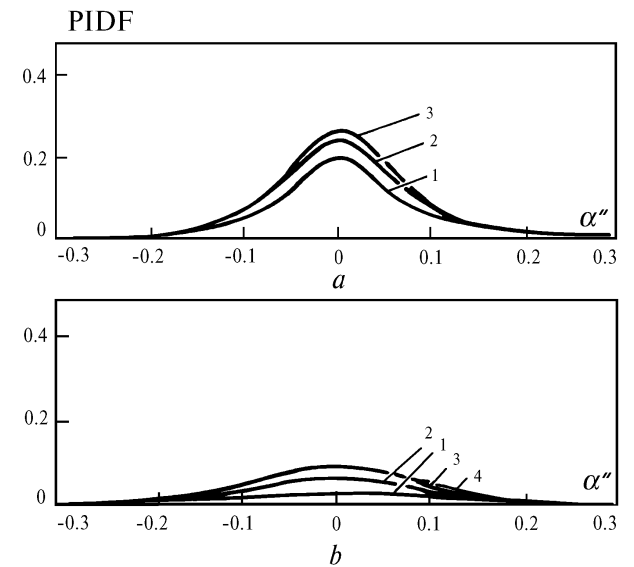
FIG. 3. PIDF value calculated using analog reconstruction of wave front: $r_0 = 20$ (a) and 10 cm (b), $N_S = 4$ (1), 16 (2), 64 (3), and 256 (4).

TABLE III.

N_S	d/r_0	St	FWHM
$r_0 = 20$ cm			
4	5/2	0.20	0.12″
4*	5/2	0.17	0.14″
16	5/4	0.24	0.14″
64	5/8	0.26	0.14″
$r_0 = 10$ cm			
4	5	0.03	0.27″
16	5/2	0.07	0.20″
64	5/4	0.10	0.19″
256	5/8	0.10	0.21″

TABLE IV.

N_{ph}	St	FWHM
1600	0.39	0.11″
800	0.28	0.12″
400	0.17	0.14″
200	0.10	0.20″

TABLE V.

N_S	N_m	St	FWHM
4	6	0.26	0.12″
16	15	0.28	0.12″
64	28	0.18	0.15″

9. EFFICIENCY OF MODAL ALGORITHM FOR RECONSTRUCTING UNDER CONDITIONS OF A PHOTON NOISE

In this section we present the results of calculation of the PIDF under conditions of presence of a photon noise in the wave−front sensor. The calculations were made for $r_0 = 20$ cm. In one case, keeping the number of subapertures of a sensor $N_S = 16$ fixed we varied the statistically mean number of photons N_{ph} (Fig. 4, Table IV), while in the other case the number of subapertures was varied at a fixed photon number $N_{ph} = 800$ (Table V). The number of polynomials being used in the algorithm of modal reconstruction of wave front was taken to be equal approximately to the number of subapertures.
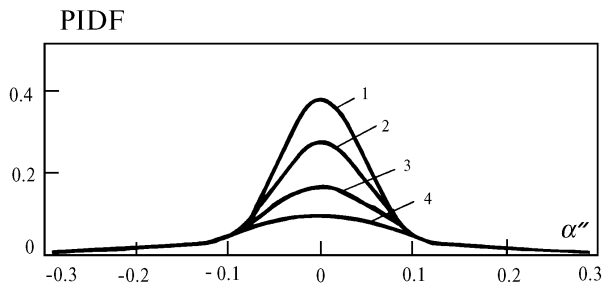
FIG. 4. PIDF value obtained with the use of a modal algorithm in the presence of quantum intensity fluctuations: $N_{ph} = 1600$ (1), 800 (2), 400 (3), and 100 (4); $r_0 = 20$ cm, $N_S = 16$, and $N_m = 15$.

Thus, approximately one hundred photons per each subaperture of the sensor are needed (in this case the subaperture size was equal approximately to the radius of coherence) during the period when the turbulence can be considered frozen, to keep the efficiency of the correction on the level corresponding to the infinite signal−to−noise ratio. For a smaller number of photons there is an optimal number of subapertures. When the number of subapertures is larger than this number, high level of noise leads to a significant increase of the measurement error of the local tilts of a wave front. In the opposite case the uncertainty in reconstruction increases as a result of insufficient spatial resolution of the sensor.

CONCLUSIONS

In this paper we have presented the results of calculations of the PIDF of an adaptive telescope with a wave front sensor of a Hartmann type and a segmented corrector that are obtained with the help of the program that could successfully used in the researches aimed at developing systems of adaptive optics, for selecting optimal configurations of a sensor and of a wave−front corrector, as well as for testing of different algorithms of controlling the corrector. The program is applicable not only to statistical simulations, in which case the radiation parameters are averaged over an ensemble of random realizations of the turbulent distortions, but also to the dynamical simulations, where time averaging is assumed. In this paper we have presented the results of statistical simulation. These results allow one to estimate the size of elements of a sensor and of subapertures of a corrector, as well as the number of photons of a reference radiation which still provides obtaining the angular resolution close to the diffraction limited value. In our model the number of elements of a corrector is equal to the number of subapertures of a sensor. It follows from the calculational results that when a modal algorithm of reconstructing a wave front is used this number of elements of the corrector is too large because the diffraction resolution can be reached using much smaller number of elements (each of which has three degrees of freedom) provided that the wave−front distortions are known.

Further investigation of the PIDF of the adaptive telescope implies carrying out dynamical modeling of the turbulent distortions of the wave front and of components of an adaptive system. This will make it possible to optimize the time of recording the signal by a wave−front sensor and to examine the algorithms for controlling the corrector and for forecasting the wave−front distortions according to the measurements done previously. The development of this computer program includes the possibility of taking into account the effects of nonisoplanarity, modeling of artificial reference sources, different types of wave−front sensors (shift interferometer, Hartmann sensor of the wave−front curvature), different types of correctors, as well as the adaptive systems with several wave−front correctors.

REFERENCES

1. V.I. Tatarskii, *Wave Propagation in a Turbulent Medium* (McCraw–Hill, New York, 1961).

2. M. Born and E. Wolf, *Principles of Optics*, 4th ed. (Pergamon Press, Oxford, 1970).

3. J.W. Goodman, *Introduction to Fourier Optics* (McGrane–Hill, New York, 1968).

4. D.L.Fried, J. Opt. Soc. Am. **56**, No. 10, 1372–1379 (1966).

5. D.L. Fried, Proc. IEEE **55**, 57–67 (1966).

6. R.J. Noll, J. Opt. Soc. Am. **66**, No. 3, 207–211 (1976).

7. N. Roddier, Opt. Eng. **29**, No. 10, 1174–1180 (1990).

8. R. Buckley, J. Atmos. Terr. Phys. **37**, 1431–1446 (1975).

9. J.M. Martin and S.M. Flatte, Appl. Opt. **27**, No. 11, 2111–2126 (1988).

10. R.C. Smithson, M.L. Peri, J. Opt. Soc. Atm. **6**, No. 1, 92–97 (1989).

11. R.C. Smithson, M.L. Peri, and R.S. Benson, Appl. Opt. **27,** No. 8, 1615–1620 (1988).

12. R.H. Hudgin, J. Opt. Soc. Am. **67**, No. 3, 375–378 (1977).

13. D.L. Fried, J. Opt. Soc. Am. **67**, No. 3, 370–375 (1977).

14. R.J. Noll, J. Opt. Soc. Am. **68**, No. 1, 139–140 (1978).

15. B.R. Hunt, J. Opt. Soc. Am. **69**, No. 3, 393–399 (1979).

16. R. Cubalchini, J. Opt. Soc. Am. **69**, No. 7, 972–977 (1989).

17. J. Herrman, J. Opt. Soc. Am. **70**, No. 1, 28–35 (1980).

18. W.H. Southwell, J. Opt. Soc. Am. **70**, No. 8, 998–1006 (1970).

19. J. Herrman, J. Opt. Soc. Am. **71**, No. 8, 989–992 (1981).

20. A.N. Bogaturov, Izv. Vyssh. Uchebn. Zaved., Ser. Fiz. **28,** No. 11, 86–95 (1985).

21. K. Freischlad and C.C. Koliopoulos, Proc. SPIE **551**, 74–80 (1985).

22. D.P. Petersen and Kyung Hyun Cho, J. Opt. Soc. Am. **3**, No. 6, 818–825 (1986).

23. Hiroaki Takajo, and Tohoru Takahashi, J. Opt. Soc. Am. **5**, No. 11, 1818–1827 (1988).